

Low temperature growth of ZnO nanotubes for fluorescence quenching detection of DNA

Faheem Ahmed¹ · Nishat Arshi¹ · Saurabh Dwivedi³ · Bon Heun Koo² · Ameer Azam³ · Edreese Alsharaeh¹

Received: 18 April 2016 / Accepted: 28 October 2016 / Published online: 14 November 2016
© Springer Science+Business Media New York 2016

Abstract In this work, large-scale and single-crystalline ZnO nanotubes were fabricated by a simple technique from an aqueous solution at a low temperature of 65 °C. According to detailed morphology, structural and compositional analyses showed that the ZnO nanotubes [diameter ~200 nm (wall thickness ~50 nm); length ~1 μm] have single-crystallite with wurtzite structure. As-prepared ZnO nanotubes showed an effective fluorescence quenching for the detection of calf thymus DNA. In particular, increasing DNA concentrations (5–50 μM) into the fixed concentration of ZnO nanotubes (50 μM) progressively quenched the intrinsic fluorescence of nanotubes, which showed that the nanotubes fluorescence was efficiently quenched upon binding to DNA. At the highest ZnO-DNA molar ratios of 1:1.8, around 50.1 % of fluorescence quenching of DNA was observed. Significance of this study provides simple, cost-effective, and low temperature synthesis of ZnO nanotubes revealed better fluorescence property toward a platform of DNA sensor.

Graphical Abstract ZnO nanotubes with diameter of ~200 nm (wall thickness ~50 nm) and length of about 1 μm prepared at low temperature (65 °C) showed fluorescence was efficiently quenched upon binding to DNA. In particular, around 50.1 % of DNA fluorescence quenching at the highest ZnO-DNA molar ratios of 1:1.8 was observed.

Electronic supplementary material The online version of this article (doi:10.1007/s10856-016-5805-3) contains supplementary material, which is available to authorized users.

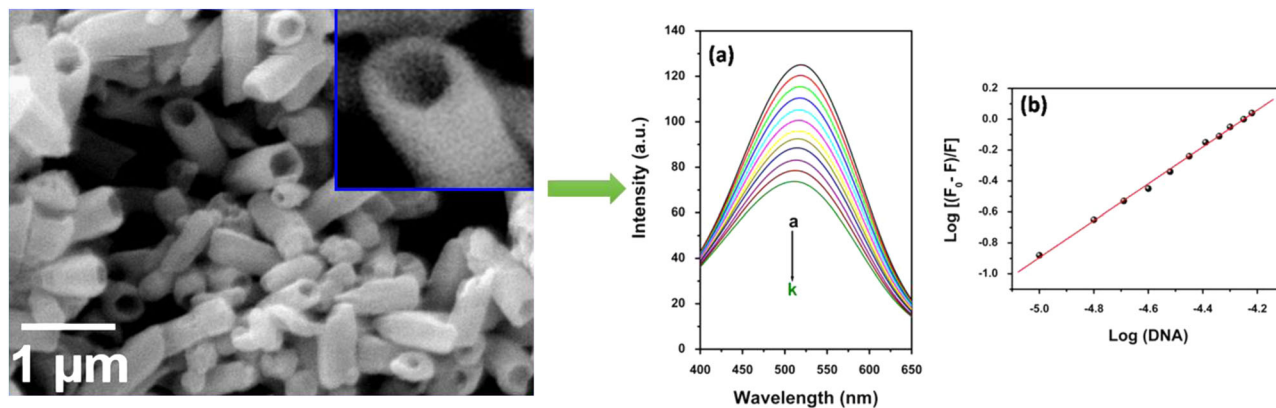
✉ Faheem Ahmed
faheem030@gmail.com

✉ Edreese Alsharaeh
ealsharaeh@alfaisal.edu

¹ College of Science & General Studies, Alfaisal University, Riyadh, Saudi Arabia

² School of Materials Science & Engineering, Changwon National University, Changwon, South Korea

³ Department of Applied Physics, Aligarh Muslim University, Aligarh, India



1 Introduction

The existence and quantity of biological markers including carbohydrates, proteins, and DNA are often essential signals of some specific disease states and physiological processes, and have a unique advantage in that they may be used for the precise and sensitive warning of damage at low levels [1]. Numerous applications of DNA detection have been found in gene expression pro-filing, clinical disease diagnostics and treatment, it is thus extremely important to develop rapid, cost-effective, sensitive and precise detection methods [1]. The increasing accessibility of nanostructures has produced extensive interest in their diagnostic application [2, 3] and a diversity of nanostructures has been successfully used for this purpose [4]. Many efforts have been made to developing fluorescence assays based on fluorescence resonance energy transfer (FRET) or quenching mechanism for nucleic acid detection [5]. The use of nanostructure as a “nanoquencher” has a notable advantage in that the same nanostructure can quench dyes of different emission frequencies, consequently, the selection issue of a fluorophore–quencher pair is eliminated from the nanostructure-involved system [5, 6].

Nowadays, one-dimensional (1D) nanostructures including nanorods, nanowires, nanobelts, and nanotubes attracted enormous interest [7–11] for the fabrication of nanoscale devices. Zinc oxide (ZnO) with a wide energy bandgap of 3.37 eV and large exciton binding energy of 60 meV at room temperature is a remarkably significant semiconductor, and has attracted enormous consideration [12]. Among the 1D nanostructures of ZnO, tube-shaped ZnO crystals have paying attention due to advantages of their larger specific surface area (SSA) with special hollow structure than that of other crystal shapes. Therefore, the tube-shaped ZnO used various applications such as dye-sensitized solar cells (DSSCs), sensors, catalysts, and

hydrogen storage [13], optoelectronics, sensors, transducers, and biomedical devices [14].

Several methods were developed to prepare ZnO nanotubes, such as hydrothermal [15–17], template-based growth [18], thermal evaporation [19], plasma-molecular beam epitaxy [20], and metalorganic chemical vapor deposition [21]. Though, to realize low temperature growth of ZnO nanotubes with controllable sizes and dimensions for large scale production is still a challenge. In comparison with other synthesis methods to obtain ZnO nanotubes, low-temperature synthesis in solution form has been realized because of its simplicity [22]. Ki-Woong Chae et al. [23] reported that nanotubes were formed when the solution was first heated at 90 °C for 3 h followed by cooling down to 60 and 50 °C and maintained for 20 h. They showed that a drastic transformation of all of the ZnO nanorods to ZnO nanotubes was observed. This shape transformation suggests that a decrease in the reaction temperature might be one of the key features which affected the ZnO crystal morphology resulted to nanotubes. However, they have designed another experiment to see the formation of the ZnO nanotubes by decreasing the growth time and temperature. In that synthesis, firstly ZnO-seeded substrate was used to grow nanocrystals at 90 °C for 3 h and then at 60 °C for 5 h, which resulted to only nanorods. In Vayssieres et al. [24] report, the formation of ZnO microtubes was explained on the behalf of a selective dissolution of the metastable polar (001) face of the ZnO microrods. According to their aging mechanism, 2 days were required to convert ZnO nanotubes from nanorods.

As compared with the Ki-Woong Chae et al. [23], low growth temperature of 65 °C and short reaction time of 2 h were used in the present work for the growth of highly crystalline ZnO nanotubes. And, long-term aging process is not required as it is necessary in Vayssieres et al. experiment [24]. Also, heating the solution at 90 °C for 3 h is

not required to form ZnO nanorods and to transform to nanotubes which make the synthesis procedure more complex. In contrast to other methods, wet chemical route offers the advantage of low cost, low processing temperatures, potential for high quality nanostructures. The procedure employed in this work was simpler than established methods, since the starting solution consisted of zinc nitrate precursor and HMT was prepared in deionized water as the solvent. In this work, ZnO nanotubes were synthesized via a low temperature (65 °C) wet chemical method using water as a solvent which is more environment friendly and cheaper than other solvent. These nanotubes were successfully used for fluorescence quenching DNA detection.

2 Materials and methods

The fabrication procedure consists of two steps: (a) preparation of seeds (nanoparticles) and (b) growth of nanotubes. In the first step, a seed solution was prepared by mixing 0.03 M sodium hydroxide in methanol, and 0.01 M zinc acetate in ethanol in a round-bottom flask at 70 °C for 2 h, when a white suspension of ZnO seeds was obtained. In the second step, a 5 ml suspension of ZnO seeds was added to an aqueous solution of hexamethylenetetramine (0.035 M) in another flask and heated to 65 °C. Then, an aqueous solution of zinc nitrate (0.5 M) was slowly injected into the flask with vigorous stirring, and the reaction was kept at 65 °C for 2 h. Finally, as-prepared ZnO nanotubes were thoroughly washed with deionized water, and dried in air at 80 °C for 24 h before characterization.

The phase purity of the as-obtained product was characterized by X-ray diffraction using a Phillips X'pert (MPD-3040) X-ray diffractometer with Cu K α radiations of 1.5406 Å operated at a voltage of 40 kV and a current of 30 mA. Morphological images were obtained using field-emission scanning electron microscopy (FESEM) by MIRA II LMH microscope. The elemental composition of ZnO was determined by energy dispersive X-ray spectroscopy (EDX, Inca Oxford, attached to the FESEM). Transmission electron microscopy (TEM) micrographs, selected area electron diffraction (SAED) pattern and high-resolution transmission electron microscopy (HRTEM) images were obtained using a FE-TEM (JEOL/JEM-2100F version) operated at 200 kV. To prepare samples for TEM examination, ZnO nanotubes were dispersed in an ethanol solution, followed by an ultrasonic treatment for 10 min. A minute drop of ZnO suspension was cast onto a carbon-coated copper grid with subsequent drying in air before transferring it to the microscope. In order to perform the phonon vibrational study of the ZnO nanotubes, micro-Raman spectrometer (NRS-3100) was used with a 532 nm solid-state

primary laser as an excitation source in the backscattering configuration at room temperature. Room temperature optical absorption spectra were recorded in the range of 200–800 nm using a UV-vis spectrophotometer (Agilent-8453). Fourier transmission infrared (FTIR) spectra of the powders (as pellets in KBr) were recorded using a Fourier transmission infrared spectrometer (Nicolet Impact 410 DSP) in the range of 4000–400 cm⁻¹ with a resolution of 1 cm⁻¹.

The fluorescence quenching titration at increasing ZnO nanotubes to ctDNA molar ratios has been performed in a continuous manner. Briefly, to a fixed concentration of ZnO nanotubes (50 μ M), increasing concentrations of ctDNA (5–50 μ M) were added in 10 mM Tris-HCl buffer at ambient temperature. Fluorescence measurements were carried out on a Shimadzu spectrofluorophotometer, model RF5301PC equipped with RF 530XPC instrument control software, using a quartz cell of 1 cm path length. The excitation and emission slits were set at 3 and 10 nm, respectively. The excitation and emission wavelengths at which the fluorescence of ZnO nanotubes recorded were 330 and 520 nm, respectively. At this wavelength range, ctDNA alone does not exhibit fluorescence. Fluorescence quenching in terms of the quenching constant was determined following the Stern–Volmer Equation [25]. The slope of the double-logarithm plot ($\text{Log} [(F_0 - F)/(F - F_\infty)]$ vs $\text{Log} [\text{ctDNA}]$ in linear range provided the number of equivalent binding sites (n) however, the value of $\text{Log} [\text{ctDNA}]$ at $\text{Log} [(F_0 - F)/(F - F_\infty)] = 0$ is equal to the negative logarithm of the binding constant (K_a) [26].

3 Results

XRD pattern of as-prepared ZnO is shown in Fig. 1, indexed as the pure hexagonal phase of ZnO and in good agreement with the reported data (JCPDS, 89–1397). It is clear from the XRD pattern that the prepared ZnO has a single-phase nature with a wurtzite structure. Further, absence of diffraction peaks related to any other impurities and the sharpness of the peaks related to ZnO indicated that the prepared ZnO nanotubes have high crystallinity.

Figure 2a, b shows the FESEM images of ZnO nanotubes synthesized by low temperature route. Figure 2a clearly shows that the as-synthesized ZnO are consisted of tube like morphology which is homogeneously dispersed without any aggregation. The nanotubes have mean diameter, wall thickness, and length of about 200, 50, and 1 μ m, respectively. Inset of Fig. 2b shows an enlarged FESEM image of a single nanotube where the clear hexagonal phase of ZnO nanotubes is visible.

Additional morphological characterization is accomplished through the TEM fitted with the SAED, as shown in Figs. 2c, d. Figure 2c shows the typical TEM image of ZnO

nanotubes. It is worth noting from TEM images that the tubes were hollow (Fig. 2c). To confirm the crystal quality and growth direction, Fig. 2d shows a representative TEM image of a single ZnO nanotube. The end of the ZnO nanotube is hollow as shown in the TEM image. The detailed atomic structure of ZnO nanotubes was characterized via HRTEM. The HRTEM image in the inset of Fig. 2d shows that the ZnO nanotubes are well crystalline with an interlunar distance of about 0.267 nm, which corresponds to the distance between the (002) planes in the ZnO crystal lattice. Moreover, the selected area electron diffraction (SAED) patterns of the ZnO nanotubes (Inset of Fig. 2d) is indexed to

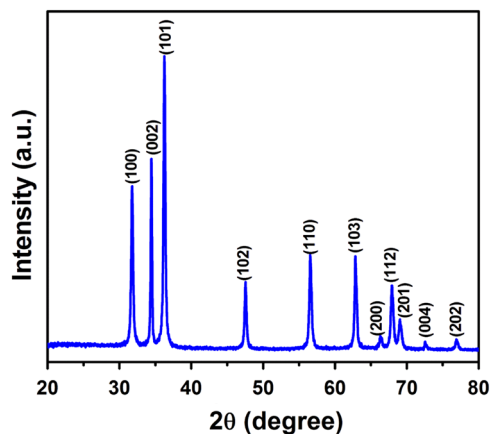
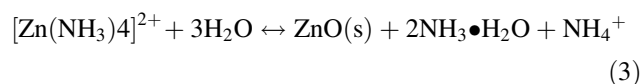
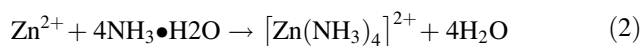


Fig. 1 XRD pattern of ZnO nanotubes prepared at low temperature

hexagonal ZnO, indicating that ZnO nanotubes are single crystalline and have growth along [0001] direction.

Generally, the wurtzite ZnO crystal has two polar planes, i.e., the (001) and (001 $\bar{1}$) planes. These two planes have high surface energy and are metastable, while the nonpolar planes parallel to the *c*-axis are the most stable planes and have a lower surface energy [24]. The growth rate of the polar (001) plane (the top plane of ZnO) is faster than that of the nonpolar planes (the lateral planes of ZnO). The following reactions might take place during the development of ZnO nanotubes:



In the beginning of the reaction scheme, the growth units in the solution near the surface of ZnO nuclei, are possibly adsorbed on the positive polar face of the (0001) surface, which resulted to the quicker growth along the [0001] direction, thus, ZnO nanorods were formed [27]. The selective deposition of colloidal Zn(OH)₂ at the edge of the (001) plane of ZnO nanorods resulting in the formation of ZnO nanotubes.

A series of exciting phenomenon were noted in successive tests by varying the growth time and temperature. The testing was intended initially to grow ZnO nanorods at

Fig. 2 FESEM images **a** low magnification, **b** high magnification of ZnO nanotubes. **c** TEM image of nanotubes in large area, **d** single nanotube, and insets show corresponding SAED and HRTEM images

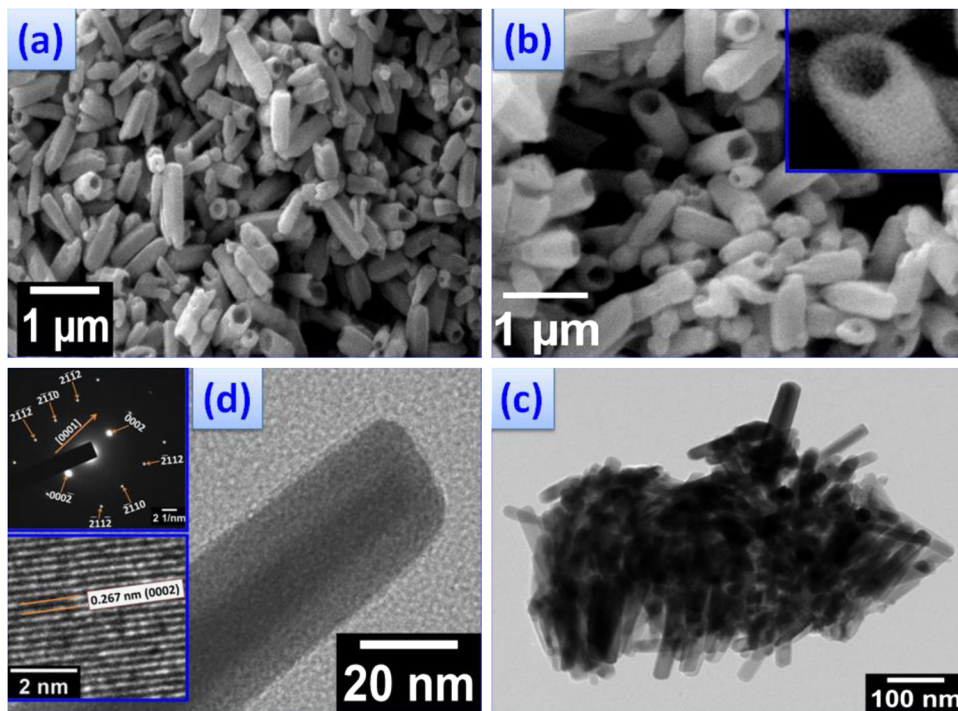
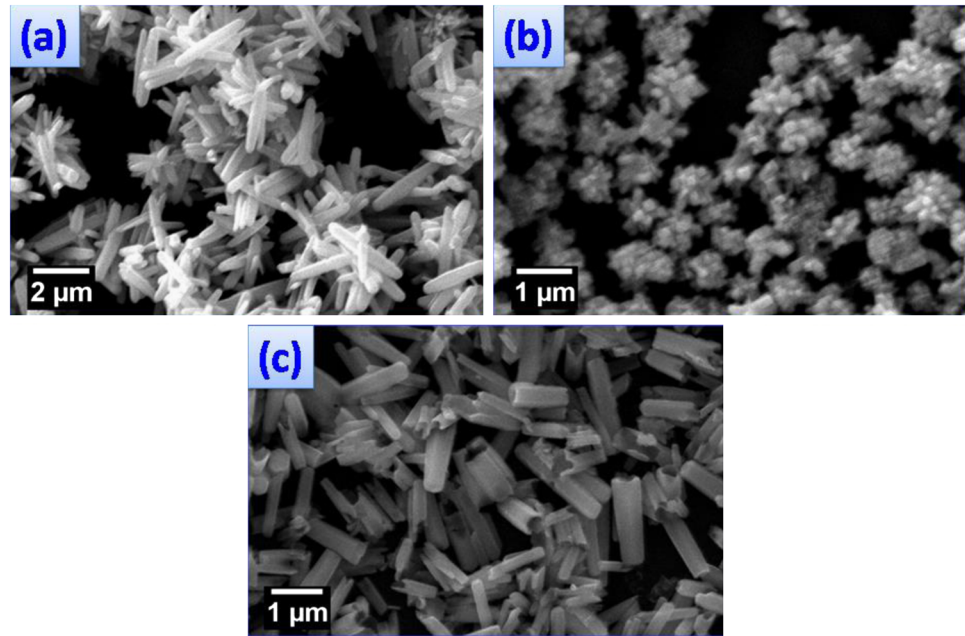


Fig. 3 FESEM images of ZnO grown at **a** 100 °C for 2 h, **b** 100 °C for 1 h, and **c** 85 °C for 2 h



100 °C for 2 h, and then was cooled down. Figure 3a shows the FESEM image of ZnO grown at 100 °C for 2 h and nanorods can be clearly seen. The ZnO grown at 100 °C for 1 h also possess rod like structure in flower shaped arrangement (Fig. 3b). Interestingly, ZnO grown at 85 °C produced mixed morphology of nanotubes and nanorods as shown in Fig. 3c. However, as shown in Fig. 2, tube-shaped ZnO nanocrystals were formed for the samples that were grown at 65 °C for 2 h. This behavior implies that the key factors that changed ZnO crystal morphology is the reduction in the reaction temperature.

A mechanism of the formation of ZnO nanotubes might be suggested as follows: The ZnO nanorods are formed at a relatively high temperature (85 and 100 °C), where the reaction solution is enriched with colloidal Zn(OH)₂ and thus permit a fast growth of ZnO nanocrystals along the [001] orientation to form nanorods [28]. A low temperature (65 °C) reaction yields a supersaturated reaction solution, resulting in an increase in the concentration of OH⁻ ions in the solution. Colloidal Zn(OH)₂ in the supersaturated solution tends to precipitate continually. However, due to a slow diffusion process in view of the low temperature and low concentration of the colloidal Zn(OH)₂, the growth of nanorods is restricted but might still occur at the edge of the nanorods due to the attraction of accumulated positive charges to those negative species in the solution, finally leading to the formation of ZnO nanotubes. Thus, the competition between the change of surface energy and growth rate dictated by the temperature can be assumed to lead to the ZnO tube structure.

In order to provide additional information on the optical properties of the as-synthesized sample, the Raman

scattering measurements were used to investigate the vibrational properties of the ZnO nanotubes at room temperature. The Raman spectra are sensitive to the crystal quality, structural defects and disorders of the grown products. It is well known that the wurtzite structure ZnO belongs to the C₄(P₆₃mc) symmetry. On the prediction of group theory, the existence of the following optical modes at the Γ point of the Brillion zone: $\Gamma_{opt} = A_1 + 2B_1 + E_1 + 2E_2$. A₁ and E₁ modes are polar and therefore split into transverse and longitudinal optical (TO and LO) components. The two are both Raman active and infrared active. The nonpolar phonon E₂ modes with symmetry are Raman active only, which have two frequencies, E₂^{high} is associated with oxygen atoms and E₂^{low} is associated with Zn sublattice, and the B₁ modes are infrared and Raman inactive (silent modes). In addition, in an ideal backscattering configuration, A₁ (TO), A₁ (LO), E₁ (TO), and E₂ modes are allowed in first-order Raman scattering when the incidence direction with respect to the crystal axis is not defined [29]. The typical room temperature Raman spectrum of the ZnO nanotubes in the range 100–800 cm⁻¹ is shown in Fig. 4. The spectrum shows a sharp, strong and dominant E₂^{high} mode of ZnO located at 437 cm⁻¹, which is the intrinsic characteristic of the Raman-active mode of wurtzite hexagonal ZnO [30]. This result is in good agreement with the XRD analysis. The peak at 334 cm⁻¹ could be assigned to the E₂^{high}-E₂^{low}, while the peak at 385 cm⁻¹ correspond to A₁(TO) phonon modes. It is generally accepted that the E₁ (LO) is related to the formation of defects in ZnO. The peak at 584 cm⁻¹ is contributed by the E₁(LO) mode of ZnO associated with the formation of defects such as oxygen vacancies or other defect states.

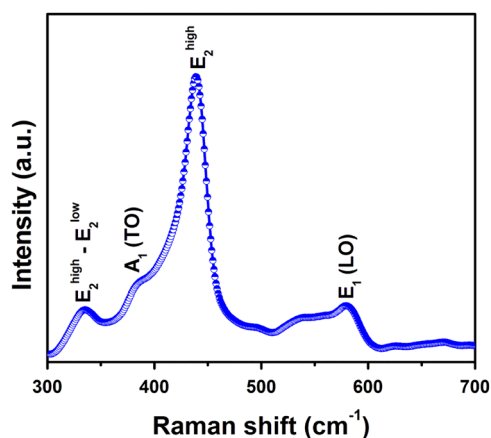


Fig. 4 Room temperature Raman spectrum of ZnO nanotubes

Therefore, the appearance of E_1 (LO) indicated that oxygen vacancies or Zn interstitials presented in the as-prepared ZnO nanotubes.

The chemical composition of ZnO nanotubes was further supported by FTIR spectrum as shown in Fig. 5. The FTIR spectra of ZnO nanotubes show main absorption bands near 3422 cm^{-1} represent O–H mode, those at 2900 cm^{-1} are C–H mode, band arising from the absorption of atmospheric CO_2 on the metallic cations at 2325 and $1400\text{--}1650\text{ cm}^{-1}$ are the C = O stretching mode. The double absorption band at 439 , and 520 cm^{-1} are assigned to Zn–O consistent with the formation on inorganic ZnO nanotubes [31].

UV–vis absorption spectrum as shown in Fig. 6, is carried out to evaluate the potential optical properties of the as-prepared ZnO nanotubes. The absorption spectrum of ZnO nanotubes show well-defined exciton band at $\sim 375\text{ nm}$ which is red shifted by $\sim 2\text{ nm}$ relative to the bulk exciton absorption (373 nm) of ZnO [32]. The red shift in the ZnO nanotube reflected a decrease in the bandgap of the semiconductor, indicating the formation of nanoscale ZnO material with similar optical properties to those reported in literature for ZnO nanostructures, nanowires, and nanobelts [33–35]. A band gap of $\sim 3.30\text{ eV}$ was obtained which is slightly smaller than the well known band gap of 3.37 eV for macrocrystalline ZnO [36, 37].

4 Discussion

The high isoelectric point (IEP) of ZnO provides a platform to immobilize DNA having low isoelectric point through electrostatic interaction. Several reports are available in literature using ZnO for biosensing purposes like, Satriano et al. [38] has reported utilization of ultrathin and nanostructured ZnO based films for fluorescence biosensing;

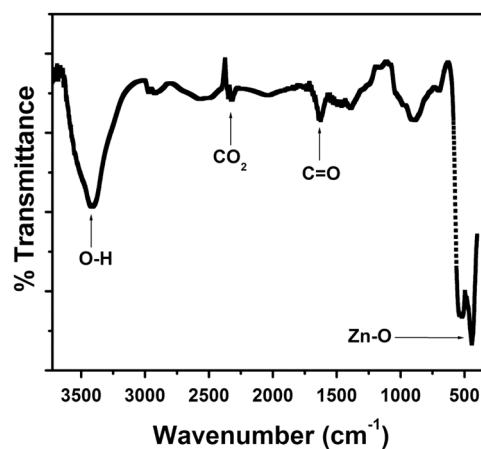


Fig. 5 FTIR spectrum of ZnO nanotubes

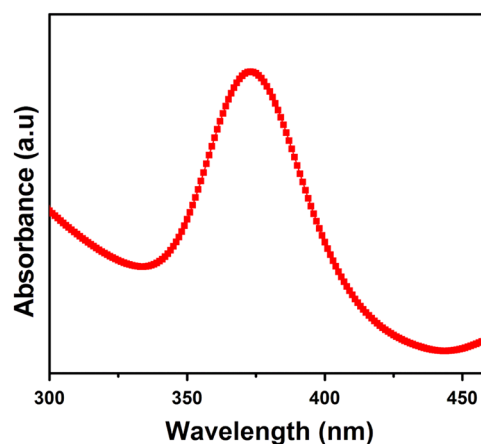


Fig. 6 UV-visible absorbance spectrum of ZnO nanotubes

Khun et al. [39] has utilized ZnO nanorods and thin films for biosensing applications and ZnO/Chitosan hybrid nanostructure based biosensor was developed by Zhao et al. [40]. ZnO nanotubes provide desirable platform for DNA to immobilize with better orientation thus, giving good stability and improved electron transfer kinetics.

Interactions of ZnO nanotubes with DNA were studied by monitoring the changes in the intrinsic fluorescence of ZnO nanotubes at varying the concentrations of DNA. Figure 7a shows the fluorescence emission spectra of ZnO nanotubes ($50\text{ }\mu\text{m}$) with the varying concentration of DNA ($5\text{--}50\text{ }\mu\text{g}$; interval of 5). Absence of DNA, ZnO nanotubes exhibit an emission maximum at 530 nm . Presence of DNA with increasing concentrations to the fixed concentration of ZnO nanotubes progressively quenches the intrinsic fluorescence of nanotubes, which shows that the nanotubes fluorescence was efficiently quenched upon binding to DNA.

A quantitative estimation of the quenching in terms of the fluorescence-quenching constant (K_{sv}) was analyzed

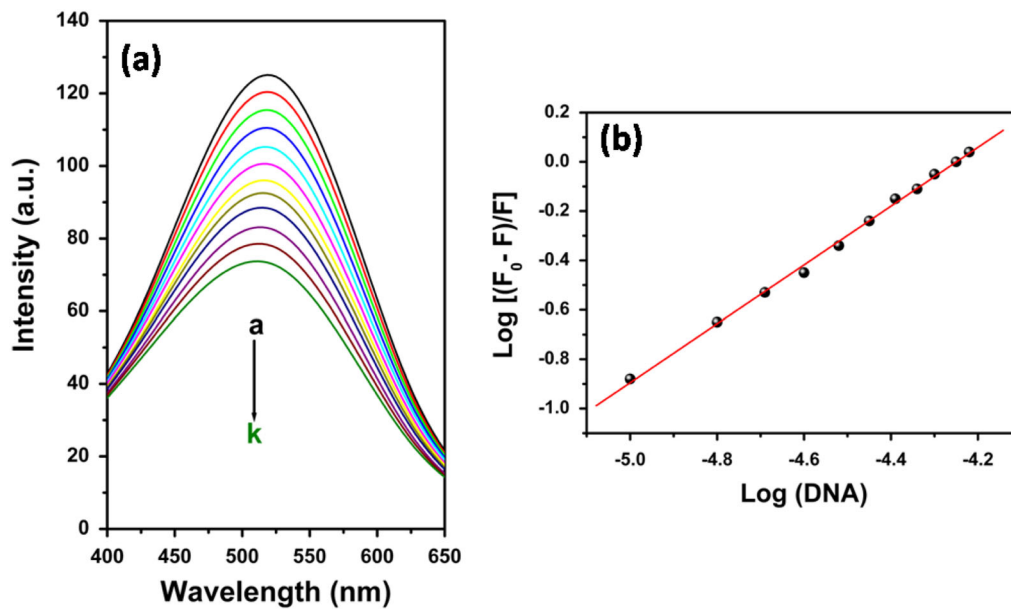


Fig. 7 Fluorescence spectra of ZnO nanotubes in the absence and presence of various concentrations of DNA; **a** emission spectra of ZnO nanotubes (50 μm) with varying DNA concentrations (5–50 μm;

increasing trend from a-k, **b** exhibits the binding isotherm of log $(F_0-F)/F$ vs. log (DNA)

using the Stern–Volmer equation [25]:

$$\frac{F_0}{F} = 1 + K_{sv}[DNA] \tag{4}$$

Where F_0 and F are the fluorescence intensities in the absence and presence of DNA, respectively, K_{sv} is the Stern–Volmer quenching constant, which is a measure of the efficiency of quenching by DNA. The titration data were used to construct a plot of F_0/F vs [DNA] and shown in Fig. 7b, and the quenching constants were obtained from the slope of the Stern–Volmer plot. The K_{sv} for ZnO nanotubes was determined for the data points falling in the linear range and the K_{sv} calculated was found to be $1.90 \times 10^4 M^{-1}$ ($r^2 = 0.99$). The plot of F_0/F vs. [DNA] drawn for ZnO nanotubes showed a linear behavior (Fig. 7b), which suggest that the quenching occurs, either static or dynamic quenching. The results exhibit around 50.1 % of DNA fluorescence quenching at the highest ZnO-DNA molar ratios of 1:1.8. Moreover, when the molecules bind independently to a set of equivalent sites on a macromolecule, the equilibrium between free and bound molecules is given by the equation mentioned below [26]:

$$\text{Log}[(F_0 - F)/F] = \text{log } K_a + n\text{log}[Q] \tag{5}$$

Where K_a is a binding constant, n is the number of binding sites. Thus, a plot of $\text{log } (F_0-F)/F$ vs $\text{log } [DNA]$ (Fig. 7b) can be used to determine K_a and n . The slope and intercept of the double-logarithm plots in linear range obtained from the experimental data of ZnO nanotubes indicated the number of equivalent binding sites (n) and

association constant (K_a). The K_a and n values for binding with DNA were determined to be $1.6 \times 10^4 M^{-1}$ and 1.2 ($r^2 = 0.99$). Consequently, from these results ZnO nanotubes prepared by low temperature route can be used as a potent platform for fluorescence quenching-based bimolecular detection assays.

The interaction of DNA with ZnO nanotubes can be well understood by the theoretical calculations using self-consistent-charge density-functional tight-binding (SCC-DFTB) method reported by Supriya et al. [41]. They showed that the calculated binding energy order and the interaction strength of DNA are dependent on the nature of the nanoparticle surfaces and also different for various morphology. In most of the cases ZnO prefers to bind either through the top site of the nucleobases or with the ring nitrogen atom having a lone pair relative to other binding sites of the bases. For nanotubes the curvature of the tube plays an important role in determining the electronic structure of the systems. Consequently, to examine the curvature effect on the adsorption of base molecules on ZnO nanotubes and they considered three single walled (SW) zig-zag ZnO nanotubes with the diameters of 1.10, 3.31, and 4.41 nm. The optimized bond lengths of Zn–O bonds in bare ZnO nanotubes were 1.88 and 1.91 Å. After adsorption of base molecules on the nanotubes surface, the Zn–O bond lengths varied from 1.88 to 1.97 Å. They considered all possible interaction sites of base molecules with ZnO nanotubes. They showed that for high curvature ZnO nanotubes the energetically most preferable interaction of the DNA to the nanotubes takes place through N-site

whereas for low curvature nanotubes take place through top site. So they concluded that the stability order very much depends on the nanotubes curvature. From the band edge wave function analysis they found that both valance band (VB) and (CB) of pristine ZnO nanotubes was delocalized over the whole nanotubes surface and independent on both diameter and the curvature of the nanotubes. But when base molecule was adsorbed on ZnO nanotubes surfaces then CB was localized on the base molecules and the VB was delocalized over the nanotubes. When the diameter of the nanotubes was small i.e curvature was high then VB was delocalized over the whole nanotubes surface but they found that for nanotubes of lower curvature, VB became localized over a particular region of nanotubes, in particular to the region close to where nucleobases were absorbed.

5 Conclusion

In summary, a simple and cost-effective method was developed for synthesize ZnO nanotubes at low temperature (65 °C). The XRD, Raman, FTIR, HRTEM, and SAED patterns confirmed the formation of wurtzite hexagonal with single crystalline ZnO nanotubes. ZnO nanotubes exhibited the red-shifted absorption at ~375 nm examined by UV–vis absorption. As-prepared ZnO nanotubes have been proven to be an effective sensing platform toward fluorescence quenching for the detection of DNA. This simple and low-cost process of ZnO nanotubes growth provides a promising route to prepare an effective DNA sensor and can be used as a universal strategy for DNA detection.

Acknowledgments This work was supported by the Internal Research Grant, Alfaisal University (IRG 2014) project No. 4050101011410. The authors gratefully acknowledge the continued support from Alfaisal University and its office of Research.

Compliance with ethical standards

Conflict of interest The authors declare that they have no competing interests.

References

- You CC, Miranda OR, Gider B, Ghosh PS, Kim I, Erdogan B, Krovi SA, Bunz UHF, Rotello VM. Detection and identification of proteins using nanoparticle–fluorescent polymer ‘chemical nose’ sensors. *Nat Nanotechnol.* 2007;2:318.
- Bunz UH, Rotello VM. Gold nanoparticle–fluorophore complexes: sensitive and discerning “noses” for biosystems sensing. *Angew Chem Int Ed.* 2010;49:3268.
- Haab BB. Applications of antibody array platforms. *Curr Opin Biotechnol.* 2006;17:415.
- Chen XQ, Zhou Y, Peng XJ, Yoon JY. Fluorescent and colorimetric probes for detection of thiols. *Chem Soc Rev.* 2010; 39:2120.
- Zhang K, Zhou HB, Mei QS, Wang SH, Guan GJ, Liu RY, Zhang J, Zhang ZP. Instant visual detection of trinitrotoluene particulates on various surfaces by ratiometric fluorescence of dual-emission quantum dots hybrid. *J Am Chem Soc.* 2011;133:8424.
- Han MY, Gao XH, Su JZ, Nie S. Quantum-dot-tagged microbeads for multiplexed optical coding of biomolecules. *Nat Biotechnol.* 2001;19:631.
- Wang ZL. Electron and ionic transport in high-radioactive silicate alkali-earth glasses. *J Phys Conds Matter.* 2004;16:829.
- Huang MH, Mao S, Feick H, Yan H, Wu Y, Kind H, Weber E, Russo R, Yang P. ChemInform Abstract: room-temperature ultraviolet nanowire nanolasers. *Science.* 2001;292:1897.
- Zhang Z, Sun YH, Zhao YG, Li GP, Wu T. Manganite thin film/ ZnO nanowire (nanosheets) p-n junctions. *Appl Phys Lett.* 2008; 92:103113.
- Kind H, Yan HQ, Messer B, Law M, Yang PD. Nanowire ultraviolet photodetectors and optical switches. *Adv Mater.* 2002;14:158.
- Li YD, Li X, He R, Zhu J, Zhao X. Artificial lamellar mesostructures to WS₂ nanotubes. *J Am Chem Soc.* 2002; 124:1411.
- Wang ZL, Kong XY, Ding Y, Gao PX, Hughes WL, Yang RS, Zhang Y. Semiconducting and piezoelectric oxide nanostructures induced by polar surfaces. *Adv Funct Mater.* 2004;14:943.
- Li QH, Gao T, Wang YG, Wang TH. Adsorption and desorption of oxygen probed from ZnO nanowire films by photocurrent measurements. *Appl Phys Lett.* 2005;86:123117.
- Wang ZL. Zinc oxide nanostructures: growth, properties and applications. *J Phys Condens Matter.* 2004;16:829.
- Vayssieres L, Keis K, Hagfeldt A, Lindquist S. Three-dimensional array of highly oriented crystalline zno microtubes. *Chem Mater.* 2001;13:4395.
- Baruah S, Dutta J. Hydrothermal growth of ZnO nanostructures. *Sci Technol Adv Mater.* 2009;10:013001.
- Yang JH, Zheng JH, Zhai HJ, Yang LL, Liu L, Gao M. Solvothermal growth of highly oriented wurtzite-structured ZnO nanotube arrays on zinc foil. *Cryst Res Technol.* 2009; 44:619.
- Wang Z, Li L. Highly ordered zinc oxide nanotubules synthesized within the anodic aluminum oxide template. *Appl Phys A.* 2002;74:201.
- Kong XH, Sun XM, Li XL, Li YD. Catalytic growth of ZnO nanotubes. *Mater Chem Phys.* 2003;82:997.
- Liang HW, Lu YM, Shen DZ, Li BH, Zhang ZZ, Shan CX, Zhang JY, Fan XW, Du GT. Growth of vertically aligned single crystal ZnO nanotubes by plasma-molecular beam epitaxy. *Solid State Commun.* 2006;137:182.
- Zhang BP, Binh NT, Wakatsuki K, Segawa Y, Yamada Y, Usami N, Kawasaki M, Koinuma H. Formation of highly aligned ZnO tubes on sapphire (0001) substrates. *Appl Phys Lett.* 2004; 84:4098.
- Feng XJ, Feng L, Jin MH, Zhai J, Jiang L, Zhu DB. Reversible super-hydrophobicity to super-hydrophilicity transition of aligned zno nanorod films. *J Am Chem Soc.* 2004;126:62–63. doi:10.1021/ja038636o.
- Chae KW, Zhang Q, Kim JS, Jeong YH, Cao G. Low-temperature solution growth of ZnO nanotube arrays. *Beilstein J Nanotechnol.* 2010;1:128–34.
- Vayssieres L, Keis K, Hagfeldt A, Lindquist SE. Three-dimensional array of highly oriented crystalline Zno microtubes. *Chem Mater.* 2001;13:4395–98.
- Lakowicz JR. Principles of fluorescence spectroscopy. 3rd ed. New York: Springer; 2006, p. 278–82.

26. Bresloff JL, Crothers DM. Equilibrium studies of ethidium-polynucleotide interactions. *Biochemistry*. 1981;20:3547–53.
27. Yu QJ, Fu WY, Yu CL, Yang HB, Wei RH, Li MH, Liu SK, Sui YM, Liu ZL, Yuan MX, Zou GY. Fabrication and optical properties of large-scale zno nanotube bundles via a simple solution route. *J Phys Chem C*. 2007;111:17521.
28. Li Y, Meng GW, Zhang LD, Phillipp F. Ordered semiconductor ZnO nanowire arrays and their photoluminescence properties. *Appl Phys Lett*. 2000;76:2011.
29. Decremps F, Ellicer-Porres J, Saitta AM, Chervin JC, Polian A. High-pressure Raman spectroscopy study of wurtzite ZnO. *Phys Rev B*. 2002;65:092101.
30. Yu WD, Li XM, Gao XD, Qiu PS, Cheng WX, Ding AL. Effect of zinc sources on the morphology of ZnO nanostructures and their photoluminescence properties. *Appl Phys A*. 2004;79:453.
31. Wahab R, Ansari SG, Kim YS, Seo HK, Shin HS. Room temperature synthesis of needle-shaped ZnO nanorods via sonochemical method. *Appl Surf Sci*. 2007;253(18):7622.
32. Yang CL, Wang JN, Ge WK, Guo L, Yang SH, Shen DZ. Enhanced ultraviolet emission and optical properties in polyvinyl pyrrolidone surface modified ZnO quantum dots. *J Appl Phys*. 2001;90:4489.
33. Wong EM, Hoertz PG, Liang CJ, Shi BM, Meyer GJ, Searson PC. Influence of organic capping ligands on the growth kinetics of ZnO nanoparticles. *Langmuir*. 2001;17:8362.
34. Spanhel L, Andersen A. Semiconductor clusters in the sol-gel process: quantized aggregation, gelation, and crystal growth in concentrated zinc oxide colloids. *J Am Chem Soc*. 1991; 113:2826.
35. Sun H, Zhang Q-F, Wu JL. Electroluminescence from ZnO nanorods with an n-ZnO/p-Si heterojunction structure. *Nanotechnology*. 2006;17:2271.
36. Huang MH, Mao S, Feick H, Yan H, Wu Y, Kind H, Weber E, Russo R, Yang P. Catalytic growth of zinc oxide nanowires by vapor transport. *Science*. 2001;292:1987.
37. Mulligan RF, Iliadis AA, Kofinas PJ. Synthesis and characterization of ZnO nanostructures templated using diblock copolymers. *Appl Polym Sci*. 2003;89:1058.
38. Satriano C, Fragala ME, Aleeva Y. Ultrathin and nanostructured ZnO-based films for fluorescence biosensing applications. *Sens Actuators B*. 2012;161:191.
39. Khun K, Ibupoto ZH, Chey CO, Lu Jun, Nur O, Willander M. Comparative study of ZnO nanorods and thin films for chemical and biosensing applications and the development of ZnO nanorods based potentiometric strontium ion sensor. *Appl Surface Sci*. 2013;268:37–43.
40. Zhao M, Huang J, Zhou Y, Chen Q, Pan X, He H, Ye Z. A single mesoporous ZnO/Chitosan hybrid nanostructure for a novel free nanoprobe type biosensor. *Biosens Bioelectron*. 2013;43: 226–30.
41. Supriya S, Pranab S. Understanding the interaction of DNA–RNA nucleobases with different ZnO nanomaterials. *Phys Chem Chem Phys*. 2014;16:15355.